# Multi-Objective Control Architecture for an Autonomous In-wheel Driven Electric Vehicle

Fadel Tarhini, Reine Talj, Moustapha Doumiati

# Multi-Objective Control Architecture for an Autonomous In-wheel Driven Electric Vehicle ⋆

**Fadel Tarhini** * **Reine Talj** * **Moustapha Doumiati** **

* *Sorbonne université, Université de Technologie de Compiègne, CNRS, Heudiasyc UMR 7253, CS 60 319, 60 203 Compiègne, France.*
** *ESEO-IREENA UR 4642, 10 Bd Jeanneteau, 49100 Angers, France.*

**Abstract:** This paper investigates the high-level control of an in-wheel-motor-drive autonomous electric vehicle. Four distinct objectives are achieved, including lateral and longitudinal control, as well as stability and maneuverability control. Actuators designated at the low level are active front steering specified for the lateral control and the 4 independent in-wheel motors for the remnant objectives. Stability and maneuverability are realized using the direct yaw control by distributing driving and braking torques among the motors, along with the longitudinal control within a torque allocation unit. In contrast to critical situations, maneuverability is promoted while relaxing the stability objective during normal driving situations. Hence, a decision layer is developed to coordinate the stabilizing and maneuvering objectives on the same actuator, thus a multi-layer Global Chassis Control (GCC) architecture is established. The control architecture is tested and validated within a MatLab/Simulink environment. Simulation results carried out on a full nonlinear vehicle model emphasize the objectives' achievement and demonstrate the superior performance of such system.

*Keywords:* Global Chassis Control; Torque Allocation; In-wheel motors, Super-Twisting Sliding Mode, Autonomous Vehicle.

## 1 Introduction

Road safety is a major issue in our community. According to the "National Highway Traffic Safety Administration", human errors contribute to more than 90% of road accidents [Rajamani (2012)]. After the development of increasingly sophisticated driver assistance systems (ADAS) to support the driver, studies are moving towards the autonomous vehicle (AV) to improve road safety and free the driver. Vehicle autonomy is accomplished in consecutive steps including perception, planning, and control. Taking perceptual data as inputs, and considering a preplanned trajectory, the objective of attaining a level of vehicle autonomy lies in controlling the lateral dynamics that ensures a trajectory following. [Tagne et al. (2016)] proposed to control the lateral acceleration to track a reference one which depends on vehicle longitudinal velocity and road curvature, while the yaw rate is controlled in [Atoui et al. (2020)] to follow a constructed reference. As an approach to couple the lateral and longitudinal dynamics, [Chebly et al. (2019)] proposed to follow a trajectory while controlling the vehicle's longitudinal velocity.

Following the global energy crisis, electric vehicles (EVs) have attracted wide range of studies in both academia and industry, owing to their ability to run entirely on renewable energy. A heavily researched category of EVs named In-Wheel-Motor-Drive EVs (IWM), have the capabilities to dominate the industry. IWM EV is an overactuated system allowing an independent control of each motor, for both traction and braking purposes. Compared with the traditional center-traction vehicle, IWM EV has shown a better performance [Zou et al. (2019)] and high potential for reducing the energy consumption [Wang et al. (2018b)]. Recently, seeking for better performance and higher efficiency, research is underway to integrate in-wheel motors into the autonomous vehicles. For the IWM AVs, [Peng et al. (2020)] proposed a robust MPC with finite time horizon for attaining path tracking while coordinating Direct Yaw Control (DYC) to minimize tire usage. [Jeong and Yim (2022)] present an integrated path tracking using pure pursuit while achieving lateral stability using DYC. An extension of the potential field method from mobile robotics to the on-road autonomous vehicle is done in [Li et al. (2017)] to minimize the lateral, longitudinal velocity and yaw angle errors for the purpose of trajectory control. The electric vehicle's control can be divided into two levels based on the structure of its actuators. Several control objectives can be ensured at the high level by intelligent coordination between the actuators at the low level, depending on diverse control strategies. A Lyapunov-based control technique is used to ensure stability and maneuverability control objectives at the high level, and realized at the low level based on a dynamic load distribution strategy in [Laghmara (2017)]. [Chokor et al. (2020)] present a comparison between a centralized approach based on $LPV/H_\infty$ and a decentralized one using Sliding Mode technique, in order to control the side-slip angle, the yaw rate and the roll angle, using DYC and Active Front Steering (AFS). Authors in [Wang et al. (2018a)] present a coordination control strategy between the differential drive assist steering (DDAS) and vehicle stability control (VSC). Control systems presented in the literature oftenly aim

⋆ This work was supported by the Agence Nationale de la Recherche (ANR)

at achieving one or two of the following objectives: lateral, longitudinal, stability, and maneuverability. In the framework of the autonomous in-wheel motor drive electric vehicle, a novel multi-layer GCC architecture is developed in this paper, considering four separate high-level objectives stated as: lateral, longitudinal, stability, and maneuverability control. A decentralized approach is adopted using the Super-Twisting Sliding Mode Control (STSMC) technique. The developed bottom-up architecture is aided with a decision layer to coordinate between stability and maneuverability. In order to distinguish the superior performance of the in-wheel vehicle, two strategies are compared for the torque distribution among the four motors. The contributions of this research work is combining the four objectives in a global integrated control architecture. Using map-matching, trajectory following is achieved by AFS. Longitudinal control assists with a comfortable drive and enhance the path tracking. A supervision layer is developed to switch between stability and maneuverability using DYC. Longitudinal, stability and maneuverability control objectives are achieved by a torque allocation strategy through the four in-wheel motors.
The rest of the paper is structured as follows. Section 2 introduce the developed GCC architecture focusing on the high-level control and presenting the contrasted strategies at the low-level. Results and their discussion are presented in Section 3, while Section 4 concludes the paper work.

## 2 Multi-Layer GCC Architecture

### *2.1 Vehicle Model*

A full non-linear model is adopted from a previous work realized in [Chokor et al. (2016)]. It consists of combining sub-models representing the vertical, lateral/longitudinal, and the wheel/road contact dynamics. The control of such system is accomplished by forcing the vehicle parameters to converge to a linear characteristics. The well-known bicycle model is used for this purpose. It is a 2 DOF dynamic model for the lateral motion of the vehicle, represented by the vehicle side-slip angle $\beta$ and the vehicle yaw rate $\dot{\psi}$. Its state-space representation is given in (1), where $\delta_c$ is the controlled steering angle subjected to the vehicle autonomous driving.

$$\begin{pmatrix} \ddot{\psi}_{bic} \\ \dot{\beta}_{bic} \end{pmatrix} = \begin{bmatrix} -\mu\frac{l_f^2 C_f + l_r^2 C_r}{I_z V_x} & \mu\frac{l_r C_r - l_f C_f}{I_z} \\ -1 + \mu\frac{l_r C_r - l_f C_f}{M V_x^2} & -\mu\frac{C_r + C_f}{M V_x} \end{bmatrix} \begin{pmatrix} \dot{\psi}_{bic} \\ \beta_{bic} \end{pmatrix} + \begin{bmatrix} \mu\frac{l_f C_f}{I_z} & \frac{1}{I_z} \\ \mu\frac{C_f}{M V_x} & 0 \end{bmatrix} \begin{bmatrix} \delta_c \\ M_z \end{bmatrix} \tag{1}$$

where $\dot{\psi}_{bic}$ and $\beta_{bic}$ are the yaw rate and the side-slip angle of the bicycle model respectively and $V_x$ is the vehicle longitudinal velocity. Parameters description and values are given in Table 1.

$$a_y \approx V_x(\dot{\psi} + \dot{\beta}) \leq \mu g \tag{2a}$$

$$\dot{\psi}_{ref,max} = 0.85\,\frac{\mu g}{V_x} \tag{2b}$$

Lateral stability can be related to the lateral acceleration $a_y$, which is limited by the road adherence. Hence, authors in Rajamani (2012) propose to maintain $a_y$ below a threshold depending on the maximal possible adherence (2a) by saturating the yaw rate $\dot{\psi}$ (2b).

### *2.2 Decentralized GCC Architecture*

The vehicle is a complex multi-variable nonlinear system, forcing its control to be extremely difficult. Centralized and decentralized control came to serve the purpose of controlling the chassis variables by one or several controllers [Chen et al. (2016)]. In the decentralized control, each variable reflecting a desired objective, is controlled independently using a single control input in a sub-controller. Whereas in the centralized control a unique controller generates the control inputs all together in order to control all the variables of interest. The control variables are all coordinated through the decision layer which anticipates the vehicle situations, thus a multilayer architecture is developed. The main idea behind developing a multi-layer control architecture is to decompose the global architecture into several layers (Fig 1). At the middle layer, control commands are generated to ensure the desired performance on the vehicle. The objectives in this work are: lateral control for trajectory following, longitudinal control by tracking a real-time defined velocity profile, and to control the stability and maneuverability of the vehicle. The developed architecture is aided with a decision layer that monitors the driving situation based on the lateral stability index (SI), to generate time-varying scheduling parameters $\lambda_{\dot{\psi}}$ and $\lambda_{\beta}$. Based on these values, the control objectives of stability and maneuverability are promoted/attenuated. In the control layer, three decentralized SISO controllers are presented to independently control the output variables $V_x, \dot{\psi}, \beta$ and the lateral error $e_y$. A full non-linear vehicle model is used to generate the vehicle's parameters including $V_x, \dot{\psi}, \beta, \dot{\beta}$, while a reference linear bicycle model is developed to assist the parameters to converge to a familiar linear characteristics ($\dot{\psi}_{bic}, \beta_{bic}, \dot{\beta}_{bic}$). A map-matching module is used to localize the vehicle on a map and determine its lateral error ($e_y$) with respect to a trajectory formed of recorded data points, and generate a speed profile $V_{x_{des}}$ based on the road curvature and a lateral acceleration criterion. At the actuator layer, the motor actuator of AFS generates a control steering $\delta_c^a$ to track $\delta_c$ (given by the control layer). The control inputs $T_m$ and $M_z$ of the longitudinal and stability/maneuverability controllers, are received by a torque allocation unit at the low level, where it generates the driving/braking torques of the four in-wheel motors.

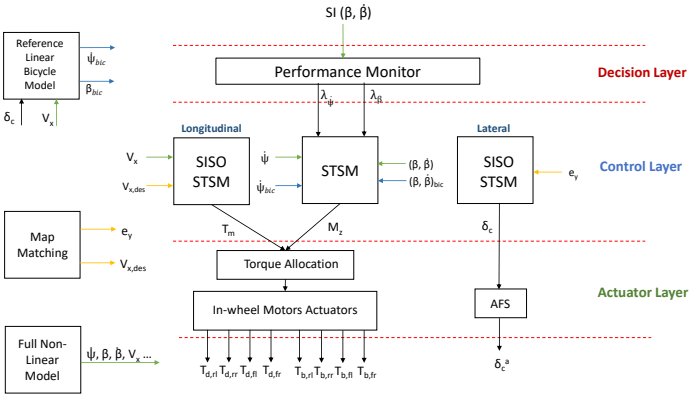


Fig. 1. Proposed GCC Architecture

### *2.3 High Level Control (Control Layer)*

The high level is composed of three decentralized controllers based on the Super-Twisting Sliding Mode Control (STSMC), that generates control inputs in order to independently control the lateral and longitudinal dynamics, and the stability/maneuverability of the vehicle.

### 2.3.1 Super-Twisting Sliding Mode Control

The Super-Twisting algorithm is a second order sliding mode control. In spite of perturbations, it generates the continuous control function that drives the sliding variable and its derivative to reach a sliding surface during a finite time.
Consider the second order system:

$$\ddot{x} = f(X,t) + g(X,t)u(t) \tag{3}$$

where $X = [x, \dot{x}]^T \in \mathbb{R}^2$ is the state vector, u is the control input, and f, g are continuous functions. $X_{des}$ is the desired state of X, with $X_{des} = [x_{des}, \dot{x}_{des}]^T \in \mathbb{R}^2$.
The error vector E is given by $E = X - X_{des} = [e, \dot{e}]^T \in \mathbb{R}^2$ where $e = x - x_{des}$ and $\dot{e} = \dot{x} - \dot{x}_{des}$.
Hence, a sliding variable with a relative degree equal to one with respect to the control input is defined :

$$s = \dot{e} + ke \tag{4}$$

The second order derivative is given by:

$$\ddot{s}(s,t) = \Phi(s,t) + \xi(s,t)\dot{u}(t), \tag{5}$$

where $\Phi(s,t)$ and $\xi(s,t)$ are bounded functions.
The goal of the Super-Twisting algorithm is to enforce the sliding variable s to converge to zero in finite time. Assume that there exist $S_0, b_{min}, b_{max}, C_0, U_{max}$ verifying that for all x $\in \mathbb{R}^n$ and $|s(x,t)| < S_0$:

$$\begin{cases} |u(t)| \leq U_{max} \\ |\Phi(s,t)| < C_0 \\ 0 < b_{min} \leq |\xi(s,t)| \leq b_{max} \end{cases} \tag{6}$$

The control input based on the Super-Twisting Sliding Mode algorithm, is given as:

$$u(t) = u_1 + u_2 \begin{cases} u_1 = -\alpha_1 |s|^{\tau} sign(s), \tau = ]0, 0.5] \\ \dot{u}_2 = -\alpha_2 sign(s) \end{cases} \tag{7}$$

where $\alpha_1$ and $\alpha_2$ are positive gains. The following conditions guarantee the finite time convergence:

$$\begin{cases} \alpha_1 \geq \sqrt{\frac{4C_0(b_{max}\alpha_2 + C_0)}{b_{min}^2(b_{min}\alpha_2 - C_0)}} \\ \alpha_2 > \frac{C_0}{b_{min}} \end{cases} \tag{8}$$

Refer to [Utkin (2013)] for the convergence analysis. An approximation function $\frac{s}{s+\epsilon}$ is used to smooth the sign(s) function, where $\epsilon > 0$.

### 2.3.2 Lateral Control

Vehicle autonomy is executed in multiple steps, starting from route planning, followed by a behavioral decision making, a motion planning and finally control. The pre-control steps fall under the decision making of the autonomous vehicle. In this work, the trajectory to be followed is modeled by a parametric curve, connecting a sequence of way-points taken from a predefined map data [Said et al. (2021)].
The lateral displacement error is computed at a look-ahead distance $L_s$ from the center of gravity of the vehicle (Fig 2). The purpose is for real-time implementation, in order to take into account the delay of the sensors and controllers/actuators. $L_s$ should be tuned as a function of the variation of longitudinal velocity and road curvature. As $V_x$ increases, this point should be further from the vehicle CG to respect the response time needed, hence $L_s$ should be increased. On the contrary, as road curvature increases, the point to be followed should be closer to the vehicle to avoid following points outside the road, hence

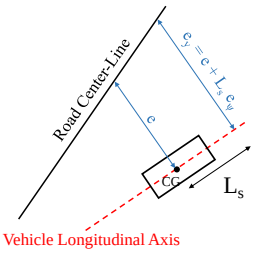


Fig. 2. Lateral error computed at a look-ahead distance $L_s$

$L_s$ should be decreased. In this work and for simplicity, $L_s$ is adapted with the longitudinal velocity variation only.
The second derivative of the lateral error can be related to the controlled steering angle as defined in [Tagne et al. (2016)] according to (9).

$$\ddot{e}_y = -\frac{C_f + C_r}{M}\beta - \frac{l_f C_f - l_r C_r}{M V_x}\dot{\psi} - \rho V_x^2 + \frac{C_f}{M}\delta_c \tag{9}$$

For the lateral control, the objective is to drive $e_y$ and its rate to zero. Let's define the sliding variable $s_y$ as (10):

$$s_y = \dot{e}_y + k_y e_y, \quad \text{with } k_y > 0 \tag{10}$$

where $s_y$ has a relative degree equal to 1 w.r.t the control input $\delta_c$ (9). Hence,

$$\ddot{s}_y(s_y,t) = \Phi_y(s_y,t) + \xi_y(s_y,t)\dot{\delta}_c(t) \tag{11}$$

$\Phi_y(s_y,t)$ and $\xi_y(s_y,t)$ are bounded functions satisfying conditions of (6). The controlled steering angle $\delta_c$ is given by

$$\delta_c = -\alpha_{\delta,1}|s_y|^{\tau_\delta} sign(s_y) - \alpha_{\delta,2}\int_0^t sign(s_y)\, d\tau, \tag{12}$$

where $\alpha_{\delta,i}$ with i = [1,2] are positive constants satisfying conditions (8). $\tau_\delta$ is a constant in the interval ]0,0.5]. The STSM control input $\delta_c$ (12) guarantees the convergence of $s_y$ to zero in a finite time, hence $\dot{e}_y + k_y e_y \to 0$. Once reaching the sliding surface, $e_y$ converges exponentially to zero with a rate $k_y > 0$.

### 2.3.3 Longitudinal Control

Longitudinal control is executed by controlling the longitudinal velocity to track a generated velocity profile. This profile adheres the speed limit of the road ($V_{x_{lim}}$) on one hand, and a comfort criterion is used, on the other hand, to keep the lateral acceleration $a_y$ under a threshold of 4 $m/s^2$ to improve vehicle stability and passenger comfort as in [Rajamani (2012)].

$$V_{x_{des}} = \min\left(\sqrt{\frac{a_{y_{max}}}{\rho}}, V_{x_{lim}}\right) \tag{13}$$

The total driving torque can be related to the longitudinal acceleration by (14) as it is defined in [Chebly et al. (2019)]

$$\begin{aligned} &M\ddot{x} - M\dot{\psi}\dot{y} + L^*\dot{\psi}^2 - \frac{T_m}{r} + \frac{4I_w\ddot{x}}{r^2} + \delta(F_{y_{fl}} + F_{y_{fl}}) = 0 \\ &L^* = l_r(m_{rr} + m_{rl}) - l_f(m_{fl} + m_{fr}) \end{aligned} \tag{14}$$

where $I_w$ is the wheel moment of inertia. The objective is to generate a total driving (traction) torque, in order to track the desired longitudinal velocity. For this purpose, let's define an error $e_x$ on the longitudinal velocity

$$e_x = V_x - V_{x_{des}} \tag{15}$$

Hence, when $e_x$ is driven to zero, $V_x$ will track $V_{x_{des}}$. So, define the sliding variable

$$s_x = e_x + k_x \int e_x \, dt \tag{16}$$

where $s_x$ has a relative degree equal to 1 w.r.t the control input $T_m$ (14), hence

$$\ddot{s}_x(s_x, t) = \Phi_x(s_x, t) + \xi_x(s_x, t)\dot{T}_m(t) \tag{17}$$

$\Phi_x(s_x, t)$ and $\xi_x(s_x, t)$ are bounded functions satisfying conditions of (6). The total driving torque $T_m$ is given by

$$T_m = -\alpha_{T_m,1}|s_x|^{\tau_{T_m}} sign(s_x) - \alpha_{T_m,2} \int_0^t sign(s_x)\, d\tau \tag{18}$$

where $\alpha_{T_m,i}$ with i = [1,2] are positive constants satisfying conditions of (8). $\tau_{T_m}$ is a constant in the interval ]0,0.5]. The STSM control input $T_m$ (18) guarantee the convergence of $s_x$ to zero in a finite time, forcing $e_x$ to converge to zero, leading to the tracking of $V_x$ to $V_{x,des}$.

### *2.3.4 Stability and Maneuverability Control*

The DYC controller has to achieve multi objectives on the same actuator, hence a decision layer has been developed to coordinate between the stability and maneuverability control objectives. The main idea is to promote one objective and attenuate the other by multiplying each sliding variable by a scheduled gain named decision variable $\lambda_i$ where $i = [\dot{\psi}, \beta]$.
The decision layer monitors the lateral stability index of the vehicle (19) as defined in [Chen et al. (2016)], and consequently generates the weighting parameters $\lambda_i$ to promote/attenuate the desired objectives based on a set of coordination rules.

$$SI = |2.49\dot{\beta} + 9.55\beta| \tag{19}$$

Let's define the state variable $X = [\dot{\psi}, \beta]^T$ and the error vector $E = [e_{\dot{\psi}}\ e_\beta]^T = [\dot{\psi} - \dot{\psi}_{ref}, \beta - \beta_{ref}]^T$ where $\dot{\psi}_{ref}$ and $\beta_{ref}$ are given in subsection (2.3.4.1). It is desired to control the yaw rate $\dot{\psi}$, the side-slip angle and its rate ($\beta$, $\dot{\beta}$), hence define the sliding variables

$$s_{\dot{\psi}} = e_{\dot{\psi}} = \dot{\psi} - \dot{\psi}_{ref} \tag{20a}$$

$$s_\beta = \dot{e}_\beta + k_\beta\, e_\beta = (\dot{\beta} - \dot{\beta}_{ref}) + k_\beta\, (\beta - \beta_{ref}) \tag{20b}$$

Since DYC is responsible for the control of the two state variables $\dot{\psi}$ and $\beta$, let's define a new sliding variable

$$s_{\dot{\psi},\beta} = c_1 s_{\dot{\psi}} + c_2 s_\beta, \tag{21}$$

where $c_1$ and $c_2$ are positive constant weights, relatively scaling the sliding variables $s_{\dot{\psi}}$ and $s_\beta$. $s_{\dot{\psi},\beta}$ has a relative degree of 1 w.r.t the control input $M_z$, hence

$$\ddot{s}_{\dot{\psi},\beta}(s_{\dot{\psi},\beta}, t) = \Phi_{\dot{\psi},\beta}(s_{\dot{\psi},\beta}, t) + \xi_{\dot{\psi},\beta}(s_{\dot{\psi},\beta}, t)\dot{M}_z(t) \tag{22}$$

where $\Phi_{\dot{\psi},\beta}(s_{\dot{\psi},\beta}, t)$ and $\xi_{\dot{\psi},\beta}(s_{\dot{\psi},\beta}, t)$ are bounded functions satisfying conditions of (6). The corrective yaw moment $M_z$ is given by

$$M_z = -\alpha_{M_z,1}|s_{\dot{\psi},\beta}|^{\tau_{M_z}} sign(s_{\dot{\psi},\beta}) - \alpha_{M_z,2} \int_0^t sign(s_{\dot{\psi},\beta})\, d\tau \tag{23}$$

where $\alpha_{M_z,i}$ with i = [1,2] are positive constants satisfying conditions of (8). $\tau_{M_z}$ is a constant in the interval ]0,0.5]. The STSM control input $M_z$ (23) guarantees the convergence of $s_{\dot{\psi},\beta}$ to zero in a finite time, hence $e_{\dot{\psi}}$ resp. $\dot{e}_\beta + k_\beta\, e_\beta$ converge to zero, meaning $\dot{\psi}$ converges to $\dot{\psi}_{ref}$ resp. $\beta$ exponentially converges to $\beta_{ref}$ with a rate $k_\beta > 0$.

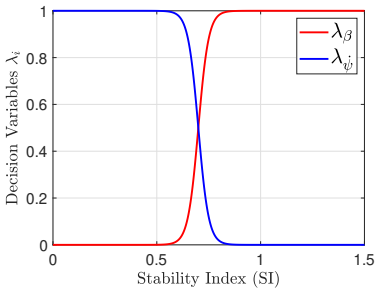


Fig. 3. Maneuverability and Stability Switching

#### *2.3.4.1 Decision Layer*

Developing a decision layer assists in switching between stabilizing and maneuvering objectives. $\lambda_{\dot{\psi}}$ and $\lambda_\beta$ vary between 0 and 1. As $\lambda_i$ approaches 1, the control objective is promoted, whereas it is attenuated at 0.
Let's define the reference control inputs as

$$\dot{\psi}_{ref} = \lambda_{\dot{\psi}}\dot{\psi}_{bic} + (1 - \lambda_{\dot{\psi}})\dot{\psi} \tag{24a}$$

$$\beta_{ref} = \lambda_\beta\beta_{bic} + (1 - \lambda_\beta)\beta \tag{24b}$$

As seen in (24), when $\lambda_i$ approaches 1, the reference variable turns into the bicycle model variable, and hence the corresponding control objective is promoted. By contrast, when $\lambda_i$ approaches 0, the reference trajectory will be the same as the actual vehicle variable, and the control objective will be relaxed accordingly.

$$s_{\dot{\psi}} = \dot{\psi} - \dot{\psi}_{ref} = \lambda_{\dot{\psi}}(\dot{\psi} - \dot{\psi}_{bic}) \tag{25a}$$

$$s_\beta = \beta - \beta_{ref} = \lambda_\beta(\beta - \beta_{bic}) \tag{25b}$$

The equivalent sliding variables in terms of the bicycle model reference are given in (25). Therefore, the state variables converge to the reference bicycle model if the corresponding decision variable is 1. Otherwise, the state variables remain without control.

#### *2.3.4.2 Coordination Rules*

Stability and Maneuverability are coordinated according to a lateral stability index criterion. For $SI < \underline{SI}$, the vehicle is in normal driving situations and no risk for instability, else, the vehicle reaches critical driving conditions and enters the instability zone, so it has to be controlled to come back to the normal driving situation before losing stability completely.
If $SI \leq \underline{SI}$, the vehicle is inside the stable zone, hence the DYC controller promotes the maneuverability control ($\lambda_{\dot{\psi}} = 1$) and turn off stability control ($\lambda_\beta = 0$). However, if the vehicle is under critical situation $SI \geq \overline{SI}$, then the DYC controller should promote the lateral stability while relaxing maneuverability.
A sigmoid function is employed for switching, to enable seamless promotion/attenuation between the low threshold $\underline{SI} = 0.6$ and the high threshold $\overline{SI} = 0.8$ (Fig 3).

$$\begin{aligned} \lambda_\beta &= \frac{1}{1 + e^{-\frac{8}{\overline{SI} - \underline{SI}}(SI - \frac{\overline{SI} + \underline{SI}}{2})}} \\ \lambda_{\dot{\psi}} &= 1 - \lambda_\beta \end{aligned} \tag{26}$$

### *2.4 Low Level Control (Actuator Layer)*

The low-level control represents the actuator layer where the desired objectives are realized by physical systems.

Table 1. Vehicle Parameters

| Symbol | Description | Value |
|---|---|---|
| $M$ | Vehicle's Total Mass | 1286.4 [kg] |
| $K_t$ | Tire stiffness coefficient | 467000 [N/m] |
| $C_t$ | Tire damping coefficient | 500 [N.s/m] |
| $t_f$ | Half front axle | 0.773 [m] |
| $t_r$ | Half rear axle | 0.773 [m] |
| $l_f$ | Distance between CG and the front axle | 1.0385 [m] |
| $l_r$ | Distance between CG and the rear axle | 1.6015 [m] |
| $I_z$ | Yaw moment of inertia | 1970 $[kg.m^2]$ |
| $g$ | Gravitational constant | 9.81 $[m/s^2]$ |
| $\mu$ | Road adherence coefficient | dry surface = 1 |
| $r$ | Wheel effective radius | 0.30759 [m] |
| $C_f$ | Front tire cornering stiffness | 76776 [N/rad] |
| $C_r$ | Rear tire cornering stiffness | 76776 [N/rad] |

Trajectory following is achieved by AFS, while the longitudinal control, along with the stability/maneuverability objectives are executed through a torque allocation among the motors. The performance of the in-wheel driven vehicle and the conventional center-traction vehicle with control systems are contrasted using two alternative approaches.

### *2.4.1 In-Wheel-Motor-Drive Vehicle*

For the in-wheel EV, $T_m$ is distributed using driving torques $T_{d_{ij}}$. The strategy is to distribute $T_m$ equally on the four motors as in (27).

$$T_{ij} = \frac{T_m}{4}, \tag{27}$$

where i,j = [r,f],[r,l] = [rear,front],[right,left].
$M_z$ is generated using half acceleration and half deceleration on the vehicle's opposite sides, using the four motors. Considering a counter-clock wise (ccw) direction and assuming small $\delta$, $M_z$ is generated using

$$\frac{M_z}{t} = -F_{x_{rl}} + F_{x_{rr}} - F_{x_{fl}} + F_{x_{fl}}, \tag{28}$$

where $t$ is the half track of the vehicle. The ratio $r/t$ is multiplied by $M_z$ to transform the moment into wheel torques, where $r$ is the wheel's radius. Each wheel on the same side receive the same torque (magnitude and direction), either braking or acceleration. Therefore, $M_z$ is generated by

$$Tb_{il} = \frac{-r}{4t} M_z \tag{29a}$$

$$Td_{ir} = \frac{r}{4t} M_z \tag{29b}$$

where $T_b$ and $T_d$ are the braking and the driving torques.

### *2.4.2 Traditional Center-Traction Vehicle*

In the traditional vehicles, a transmission system is used to distribute torques on the rear wheels via a gearbox. The traditional vehicle approach on control is widely used in literature as in [Doumiati et al. (2013), Chokor et al. (2020)].

$$T_{ri} = \frac{T_m}{2} \qquad \text{i} = [\text{r,l}] \tag{30}$$

The total driving torque is distributed equally on both of the rear wheels as in (30) while the generation of the yaw moment is achieved through Active Differential Braking (ADB) as in (31) considering a ccw direction.

$$\begin{aligned} Tb_{rl} &= \frac{-r}{t} M_z \\ Tb_{rr} &= 0 \end{aligned} \tag{31}$$

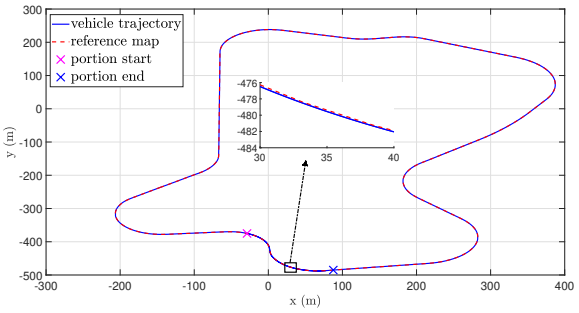


Fig. 4. Trajectory Following (Lateral Control)

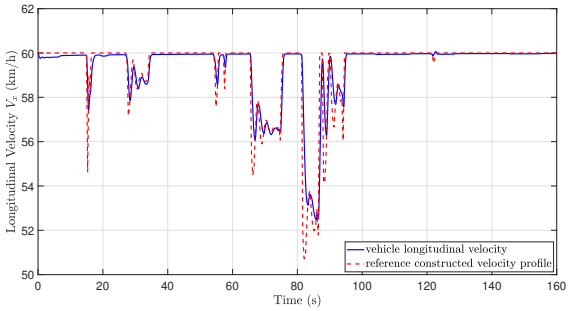


Fig. 5. Longitudinal Velocity Control - Scenario 1 (Sc1)

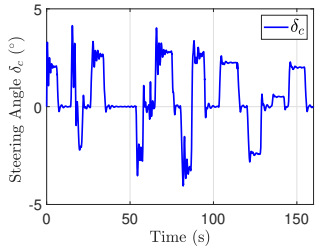


Fig. 6. Steering angle - Sc1

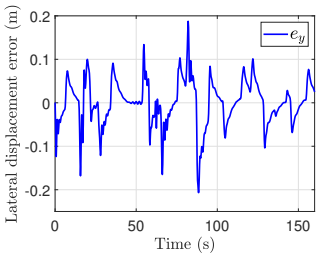


Fig. 7. Lateral error - Sc1

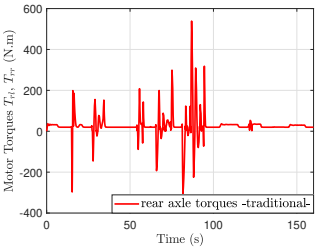


Fig. 8. Driving Torques - Sc1

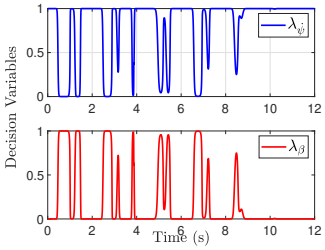


Fig. 9. Decision Variables-Sc2

## 3 Results and Discussion

The decentralized architecture is implemented and validated within Matlab/Simulink on a full non-linear model. The autonomous vehicle controlled by the AFS angle $\delta$ (Fig. 6), has shown an almost perfect tracking of the desired trajectory (Fig. 4) with a small displacement error (Fig. 7). Lateral control is tested by inducing disturbances and it results in a robust behaviour. The first scenario (Sc1) corresponds to the vehicle tracking the whole trajectory. Longitudinal control is achieved through the distribution of the driving torques for the traditional vehicle (Fig. 8) (half the magnitude for the in-wheel vehicle). Longitudinal velocity of the vehicle is observed to track the reference constructed velocity profile (Fig. 5), with smooth variations to avoid excessive longitudinal acceler-

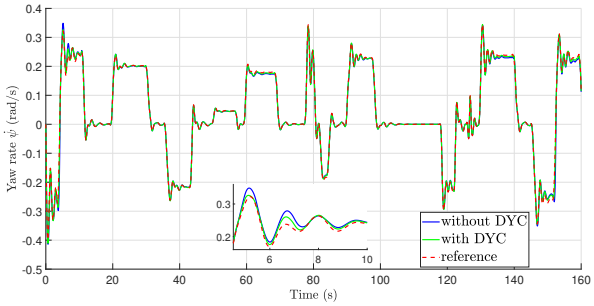


Fig. 10. Vehicle Yaw Rate - Sc1

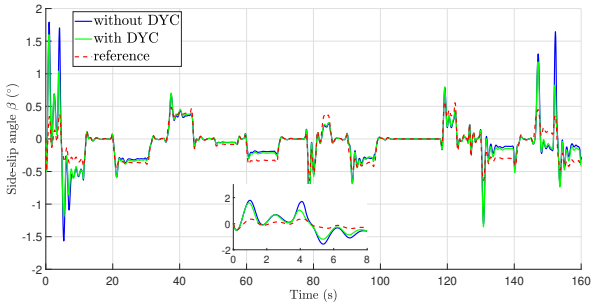


Fig. 11. Vehicle Side-slip angle - Sc1

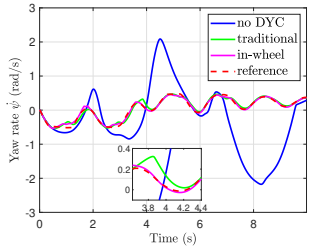


Fig. 12. Yaw rate - Sc2

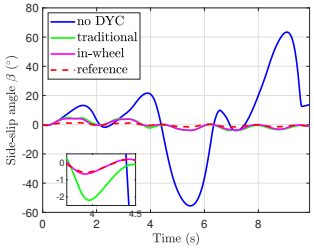


Fig. 13. Side-Slip angle - Sc2

ation. Lateral control assisted by comfortability through longitudinal control, is accompanied by the stability and maneuverability control objectives. Under the same test conditions, due to the relatively low reference velocity, the open-loop system -represented by the controlled vehicle without activating DYC- is coherent with the reference bicycle model. Hence, although there is no significant errors on the yaw rate (Fig. 10) and the side-slip angle (Fig. 11), activating DYC has enhanced the maneuverability and the stability by reducing their correspondent errors with the bicycle model. In this case, no risk on stability has been detected, so DYC has promoted only maneuverability objective.

To distinguish the effect of DYC in critical situations, a second scenario is introduced (Sc2), where a test is performed with augmenting the desired velocity (to 70 $km/h$) on the portion indicated on the map, representing a high curvature corner. Maneuverability and stability are switched according to the decision variables in (Fig. 9). We observe a major attenuation of the errors on the yaw rate and the side-slip angle (Figures 12, 13). The performance of the in-wheel driven vehicle in achieving the demanding objectives is observed to be supreme to that of the traditional vehicle. The mentioned objectives are achieved through the braking torques for the traditional vehicle (Fig. 14-left)), with a vital attenuation for that of the in-wheel driven vehicle (Fig. 14-right).

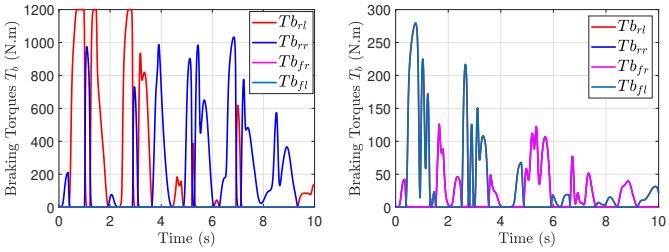


Fig. 14. Braking Torques Traditional(a), In-wheel(b) - Sc2

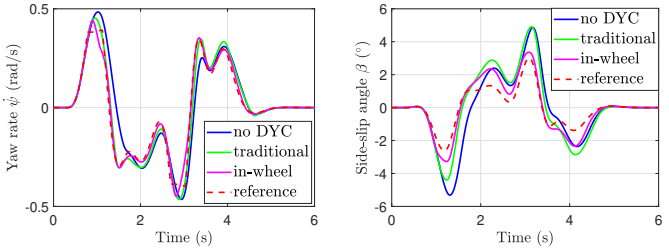


Fig. 15. Yaw rate and Side-slip angle under DLC - Sc3

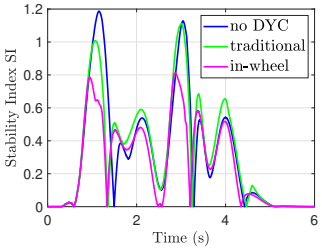


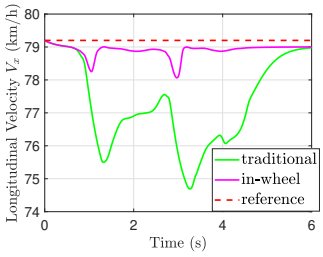


Fig. 16. Stability Index - Sc3 Fig. 17. Longitudinal Velocity

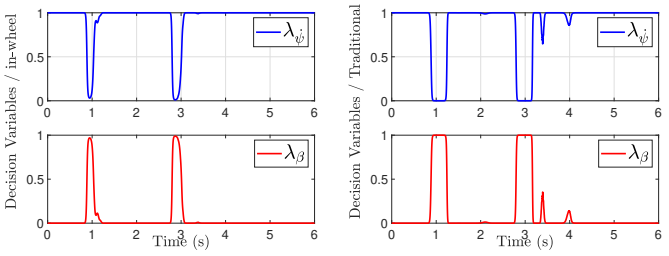


Fig. 18. Decision Variables DLC - Sc3

The last scenario (Sc3) represents a double lane change (DLC) test performed at 22 $m/s$, to distinguish the performance of the two vehicles. Maneuverability and stability reflected by the yaw rate and the side-slip angle can be observed in (Fig. 15). $\dot{\psi}$ of the in-wheel driven vehicle has shown a better performance than the traditional one, in tracking the reference bicycle model; Similarly for $\beta$. The lower stability index for the in-wheel vehicle (Fig. 16) resulted in promoting often the maneuverability objective through the decision variables. Consequently, the side-slip angle is attenuated. On the contrary to the traditional vehicle, where the decision variables indicate that it needs more time than the in-wheel vehicle to restore stability, leading to an inversely proportional behaviour (Fig. 18). Furthermore, as a result of ADB, traditional vehicles are penalized in longitudinal dynamics. Fig. 17 explicitly shows the longitudinal dynamics conservence for the in-wheel vehicle, counter to the traditional vehicle. Avoiding longitudinal velocity loss involves averting adding traction torques to compensate for the error in longitudinal velocity. As a direct consequence, stability loss is avoided,

and the vehicle is more accurately represented by the bicycle model, thus leading to lower stability index. As a result, lower $SI$ frequently promotes maneuverability. This demonstrates the premier advantage of conserving the longitudinal velocity in the in-wheel vehicles. In light of this, the in-wheel driven vehicle has shown a superior performance in achieving the desired objectives.

## 4 CONCLUSION

In this paper, a mulit-layer decentralized GCC architecture is developed for lateral, longitudinal, stability, and maneuverability control. The STSMC technique is used to develop a high-level control that comprises the desired objectives. The architecture is aided with a decision layer to switch between the stability and maneuverability objectives according to driving situations. Two strategies are approached at the low level to distinguish the primary advantage of the in-wheel-motor driven vehicles. Following the tendency of the autonomous in-wheel EV for energy economy, an energy efficient strategy for torque allocation is among the work perspectives of this study.


## Acknowledgements

This work is carried out within the framework of the V3EA project "Electric, Energy Efficient and Autonomous Vehicle" (2021-2025), funded by the French National Agency (ANR).


## References


Atoui, H., Milanés, V., Sename, O., and Martinez, J.J. (2020). Design and experimental validation of a lateral lpv control of autonomous vehicles. In *2020 IEEE 23rd International Conference on Intelligent Transportation Systems (ITSC)*, 1–6. doi:10.1109/ITSC45102.2020.9294459.

Chebly, A., Talj, R., and Charara, A. (2019). Coupled longitudinal/lateral controllers for autonomous vehicles navigation, with experimental validation. *Control Engineering Practice*, 88, 79–96. doi:10.1016/j.conengprac.2019.05.001.

Chen, W., Xiao, H., Wang, Q., Zhao, L., and Zhu, M. (2016). *Integrated vehicle dynamics and control*. doi:10.1002/9781118380000.

Chokor, A., Talj, R., Charara, A., Shraim, H., and Francis, C. (2016). Active suspension control to improve passengers comfort and vehicle's stability. In *2016 IEEE 19th International Conference on Intelligent Transportation Systems (ITSC)*, 296–301. doi:10.1109/ITSC.2016.7795570.

Chokor, A., Talj, R., Doumiati, M., Hamdan, A., and Charara, A. (2020). A comparison between a centralized multilayer l p v / h and a decentralized multilayer sliding mode control architectures for vehicle's global chassis control. *International Journal of Control*, 95, 1–32. doi:10.1080/00207179.2020.1791360.

Doumiati, M., Sename, O., Dugard, L., Martinez-Molina, J.J., Gaspar, P., and Szabo, Z. (2013). Integrated vehicle dynamics control via coordination of active front steering and rear braking. *European Journal of Control*, 19(2), 121–143.

Jeong, Y. and Yim, S. (2022). Integrated path tracking and lateral stability control with four-wheel independent steering for autonomous electric vehicles on low friction roads. *Machines*, 10(8). doi:10.3390/machines10080650. URL https://www.mdpi.com/2075-1702/10/8/650.

Laghmara, H. (2017). Yaw moment lyapunov based control for in-wheel-motor-drive electric vehicle. volume 50. doi:10.1016/j.ifacol.2017.08.2189.

Li, B., Du, H., and Li, W. (2017). A potential field approach-based trajectory control for autonomous electric vehicles with in-wheel motors. *IEEE Transactions on Intelligent Transportation Systems*, 18(8), 2044–2055. doi:10.1109/TITS.2016.2632710.

Peng, H., Wang, W., An, Q., Xiang, C., and Li, L. (2020). Path tracking and direct yaw moment coordinated control based on robust mpc with the finite time horizon for autonomous independent-drive vehicles. *IEEE Transactions on Vehicular Technology*, 69(6), 6053–6066. doi:10.1109/TVT.2020.2981619.

Rajamani, R. (2012). *Vehicle Dynamics and Control*. Springer, 2e edition. doi:10.1007/0-387-28823-6.

Said, A., Talj, R., Francis, C., and Shraim, H. (2021). Local trajectory planning for autonomous vehicle with static and dynamic obstacles avoidance. In *2021 IEEE International Intelligent Transportation Systems Conference (ITSC)*, 410–416. doi:10.1109/ITSC48978.2021.9565109.

Tagne, G., Talj, R., and Charara, A. (2016). Design and comparison of robust nonlinear controllers for the lateral dynamics of intelligent vehicles. *IEEE Transactions on Intelligent Transportation Systems*, 17(3), 796–809. doi:10.1109/TITS.2015.2486815.

Utkin, V. (2013). On convergence time and disturbance rejection of super-twisting control. *IEEE Transactions on Automatic Control*, 58(8), 2013–2017. doi:10.1109/TAC.2013.2251812.

Wang, J., Luo, Z., Wang, Y., Yang, B., and Assadian, F. (2018a). Coordination control of differential drive assist steering and vehicle stability control for four-wheel-independent-drive ev. *IEEE Transactions on Vehicular Technology*, 67(12), 11453–11467. doi:10.1109/TVT.2018.2872857.

Wang, Z., Qu, C., Zhang, L., Xue, X., and Wu, J. (2018b). Optimal component sizing of a four-wheel independently-actuated electric vehicle with a real-time torque distribution strategy. *IEEE Access*, 6, 49523–49536. doi:10.1109/ACCESS.2018.2801564.

Zou, Y., Guo, N., and Zhang, X. (2019). An integrated path-following and yaw motion control strategy for autonomous distributed drive electric vehicles with differential steering. In *2019 IEEE Intelligent Vehicles Symposium (IV)*, 1987–1992. doi:10.1109/IVS.2019.8813833.